Revision 1, #5571

Mineralogy of paloverde (*Parkinsonia microphylla*) tree ash from the Sonoran desert: a combined field and laboratory study

Laurence A.J. Garvie, School of Earth and Space Exploration, Arizona State University, Tempe, AZ 85287-6004. lgarvie@asu.edu

Abstract

In this study is described the wood chemistry and ash mineralogy of the desert tree *Parkinsonia microphylla* (Torr.) and follows the mineralogical effects of natural and laboratory aging and weathering. Ash was collected in the field (field ash) following a wildfire east of Phoenix, Arizona, May 8th, 2011, and its mineralogy compared with ash produced under laboratory conditions (laboratory ash): twenty-five minerals were identified by powder x-ray diffraction (XRD) in the fresh and weathered ash. In order to guide the interpretation of the XRD patterns, the major ash-forming elements (for elements of Na and heavier) in the wood were determined by particle-induced x-ray emission (PIXE) spectroscopy. Mg (816 to 3677 ppm), K (3965 to 17,581 ppm), and Ca (935 to 61,772 ppm) were the dominant metals, and P (to 1528 ppm), S (to 1024 ppm), and Cl (318 to 2648 ppm) were the dominant non-metals. In general, smaller branches and bark showed higher concentrations of ash-forming cations than mature wood. Powder XRD patterns from fresh field ash were dominated by various proportions of fairchildite ($K_2Ca(CO_3)_2$), calcite ($CaCO_3$), lime (CaO), bütschliite (dimorph of fairchildite), and periclase (MgO), with traces of other K-bearing salts. Following gentle rains (total 0.7 cm) at the end of May, a brittle ash crust formed which was dominated by calcite, with variable amounts of fairchildite, sylvite (KCl), kalicinite ($KHCO_3$), magnesian calcite ($(Ca,Mg)CO_3$), magnesite ($MgCO_3$), $K_2CO_3.1.5H_2O$, and arcanite (K_2SO_4). Further exposure to rain (total of 7 cm) in July and August left an ash dominated by calcite, magnesian calcite, and periclase. Ash collected two years after forming was dominated by calcite, magnesian calcite, and minor nesquihonite ($MgCO_3.3H_2O$). The mineralogy of ash produced in the laboratory from wood collected in the fire zone was dependent on the diameter and hence age of the wood. Ash from thin branches was dominated by calcite and fairchildite, consistent with the high Ca revealed by PIXE. Ash from large logs was dominated by fairchildite, with reflections from nine additional minerals including KOH, K_2CO_3, and periclase: the mineralogy is consistent with high K as determined by PIXE. KOH and K_2CO_3 disappeared within a few hours exposure to air and peaks for baylissite ($K_2Mg(CO_3)_2.4H_2O$), $K_4H_2(CO_3)_3 1.5H_2O$, and $K_2CO_3.1.5H_2O$ appeared. Further washing with water left periclase and

magnesian calcite. The mineralogical changes observed through natural and laboratory weathering show that fairchildite rapidly weathers to calcite and magnesian calcite, with solubilization and removal of K. Despite the initial mineralogical complexity, the weathered ash is consistent with that found in anthropogenic ash deposits, which is dominated by calcite. Periclase is unaffected by the relatively short-term laboratory weathering, however it was largely absent in field ash collected two years after the fire. Periclase is commonly reported from wood ash, and this study suggests an important role for biomass burning in Mg cycling.

INTRODUCTION

Biomass combustion recycles the atmospherically derived carbon, which is bound primarily as organic plant material, back into the atmosphere as CO_2. This simple cyclic model can be thought of as a net zero sequestration process as the carbon release is coupled with vegetation regrowth. However, this model does not take into account production of inorganic C-rich ash with long terrestrial residence times. Ash is an often over-looked trap of atmospherically bound CO_2, which is typically on the order of a few weight percent (wt%) of the biomass and commonly dominated by Ca and Mg oxides and carbonates (Etiégni and Campbell, 1991; Humphreys et al., 2004; Liodakis et al., 2005; Milton and Axelrod, 1947; Ulery et al., 1993; Yusiharni and Gilkes, 2012). In addition, the ash contributes to the soil chemistry, which is important in determining the quantity of organic carbon stored in soil, its turnover time, and long-term carbon fluxes (Torn et al., 1997), and affects soil properties and influences nutrient uptake by plants, e.g., (Demeyer et al., 2001; Ulery et al., 1993). For example, Ulery et al., (1993) found high pH values in wood ash and surface soil “caused by K and Na oxides, hydroxides, and carbonates.”, though these compounds are rapidly removed by rain, the soil pH remained high for several years as a result of the persistence of the wood-ash calcite. In general though, the nutrient and chemical effects on soil of moderate burning are considered to be short-lived (Chandler et al., 1983). Worldwide, anthropogenic ash production from bioenergy-produced combustion of biomass is estimated to be ~476 million tons (Vassilev et al., 2013a). However, the quantities of natural ash formation are poorly constrained, but likely significant. For example, up to 81.9 t/ha of ash were reported following wildfires in eucalypt forests in Australia (Santín et al., 2012). Worldwide, on the order of 3×10^6 km^2 of land are burned (Alonso-Canas and Chuvieco, 2015), with an estimated ~10^{10} metric tons of biomass combusted. Despite the large quantities of biomass ash produced, there are relatively few studies that describe ash mineralogy at a plant species level (Arthur et al., 1999; Liodakis et al., 2005; Wang and Dibdiakova, 2014; Yusiharni and Gilkes, 2012).

Recently formed ash is primarily light, formless powder that is rapidly distributed by wind and altered by rain. However, rock-like ash clinkers also form: first described in 1929 in burnt hollow snags in western hemlock (*Tsuga heterophylla*) (Englis and Day, 1929), they have since been more widely discovered (Humphreys et al., 2004; Humphreys et al., 2003; Milton and Axelrod, 1947). These clinkers, also called wood-ash stones, can reach in excess of 20 kg through a process called pyro-biomineralization (Humphreys et al., 2003). Clinkers from several locations have similar compositions being dominated by fairchildite ($K_2Ca(CO_3)_2$) (Milton and Axelrod, 1947) and calcite (Humphreys et al., 2004). Ash can also form crusts that affect soil surface properties, e.g., (Balfour et al., 2014) and can be preserved over archaeological time scales, e.g., (Schiegl et al., 1996; Shahack-Gross and Ayalon, 2013). Fresh ash prior to ageing is dominated by formless micron and submicron-sized particles, some with flow-like morphologies (Wang and Dibdiakova, 2014; Werkelin et al., 2011; Yusiharni and Gilkes, 2012). Ash concentrations are typically up to 5 wt% of the standing biomass, e.g., (Yusiharni and Gilkes, 2012), though some plant material, such as straw, can have significantly higher ash masses, e.g., to 18.5 wt% (Thy et al., 2013).

Ash produced during biomass combustion is mineralogically complex, with around 300 compounds identified in fresh and aged materials (Vassilev et al., 2013a; Vassilev et al., 2013b). However, ash formed during natural biomass burning has a more restricted mineralogy dominated by oxides, carbonates, and chlorides of Ca, Mg, and K (Liodakis et al., 2005; Misra et al., 1993; Yusiharni and Gilkes, 2012). Calcite is often reported as the dominant mineral following natural biomass burning (Humphreys et al., 1987; Ulery et al., 1993). The mass of ash and its mineralogy is complexly related to a range of variables such as burn temperature, combustion degree, plant age, and concentrations of the primary ash-forming elements (Liodakis et al., 2005; Miles et al., 1995; Wang and Dibdiakova, 2014; Werkelin et al., 2011; Werkelin et al., 2010). The concentrations of ash-forming elements is further dictated by the species of plant and the part of the plant combusted (Liodakis et al., 2005; Wang and Dibdiakova, 2014; Werkelin et al., 2011; Werkelin et al., 2010; Yusiharni and Gilkes, 2012). Ash mineralogy has largely been studied under controlled laboratory conditions, with only a few studies relating wood chemistry to ash mineralogy (Wang and Dibdiakova, 2014; Werkelin et al., 2011; Werkelin et al., 2010).

Fundamental to revealing the environmental consequences of ash is the species-level understanding of plant ash and its transformation over time. To this end is described the wood chemistry and ash mineralogy of the common Sonoran desert tree *Parkinsonia microphylla* (Torr.). Ash mineralogy is compared between those produced from combustion of plant materials in the laboratory and

from material collected following a wildland fire. Also investigated are the mineralogical effects of natural and laboratory aging and weathering.

MATERIALS AND METHODS

Field Ash

The Picket fire (centered around 33.27° N, 111.18° W) was reported at 11:39 am, Sunday, May 8th, 2011 on the Tonto National Forest near Boyce Thompson Arboretum, Arizona. The fire was contained on May 10th having consumed 1336 acres of the Arizona Upland subdivision of the Sonoran Desert. Visually, this landscape is dominated by legume trees (*Parkinsonia microphylla* and *Prosopsis juliflora*) and the iconic saguaro cactus (*Carnegiea gigantea*). This region is floristically lush because of the bi-seasonal rainfall pattern, bringing an average of 43 cm of rain per annum. However, at the time of the fire, this area was under a severe drought, with only 27 cm recorded from May 2010 until the start of the fire. The burn area occupies both canyon lands and steep terrain cut by Arnett Creek and Alamo Canyon. The extreme dryness at the time of the fire caused the locally abundant tree *Parkinsonia microphylla* (commonly called foothill paloverde) (Fig. 1a) as well as much of the other flora in the fire zone to burn and produce localized accumulations of ash. The paloverde is typically a small tree, with yellowish-green bark, small drought deciduous leaves, and cream-colored wood (Fig. 1b). This tree is locally common in the Sonoran desert of Arizona and south into Mexico, and is common throughout the burn site.

The first ash samples (hereafter referred to as field ash) were collected on May 15th from two trees, Tree 1 (Fig. 1c) and Tree 2. Both trees were multi-stemmed with a trunk diameter near 25 cm. Ash was collected above ground from within the hollowed-out burnt stems and stumps. The trees were still smoldering and the ash formed sometime on or after the fire started on the 8th of May. Gentle rains (0.7 cm, May 19th) wet the ash near the end of May. There was no recorded precipitation in June. Rainfall totals, recorded at nearby Boyce Thompson Arboretum, for the following months, July to December 2011, were 4.5, 2.8, 2.6, 1.3, 2.6, and 6.8 cm, respectively. Ash was collected primarily within log and stump hollows above the ground so as to not contaminate the ash with soil minerals. During 2011, paloverde ash was collected on the following dates, 15th , 24th , and 29th of May, 4th and 5th of June, 14th of July, 16th of August, and 10th of December , and then a few samples were collected in 2012 and 2013. By 2013, ash was restricted to burnt tree hollows.

Laboratory Ash

Ash was prepared in the laboratory (hereafter called laboratory ash) from wood of two paloverde trees (Tree A and B) through open-air combustion. Tree A

is medium-sized (~3 m high) growing on a low hill in the burn zone. Two sections of tree were collected – 3-cm-diameter branch (called PV1, where PV is short for paloverde) and a 9-cm-diameter green main branch (called PV2, Fig. 1b). Tree B was a large, mature individual in Alamo Canyon that was largely unburnt but killed by the fire. A 30-cm-diameter log was taken from the main trunk (called PV3).

Ash from Tree A and B were produced under smoldering conditions. Multiple ash samples prepared from different parts of Tree A and B logs and twigs. Prior to burning, the cut pieces were dried for one week in an oven set to 50° C. Approximately 300 to 500 g of dried wood, cut into <5 cm pieces, was lit uncovered in air and allowed to burn under flaming conditions. The fire was initiated for ~10 minutes with a propane burner. Thereafter, the propane burner was extinguished and flaming persisted for ~ ½ hour producing chunks of char, which then smoldered unassisted for between one and two hours leaving a predominantly white to grey ash (Fig. 1d). The temperature during smoldering was measured with an Amprobe IR-720 20:1 IR thermometer. Following cessation of flaming, spot temperature readings were taken over the smoldering wood. Each ash sample was divided into two portions. The first was transported while hot in sealed containers under low vacuum (~200 torr) to a dry nitrogen box and stored until needed for analysis. A second portion was stored unsealed in air in order to follow possible mineralogical changes with atmospheric exposure.

Proton-induced x-ray emission

Nondestructive elemental analysis of wood was undertaken by proton-induced x-ray emission (PIXE) spectroscopy. PIXE is ideally suited for elemental analysis of wood as unprepared, other than a clean surface, pieces can be analyzed (Calva-Vázquez et al., 2006; Garvie et al., 2015; Martins et al., 1999; McClenahen et al., 1989). Compared to electron-based x-ray techniques, such as energy dispersive spectroscopy (EDS), PIXE offers superior signal-to-noise ratios and hence higher trace-element sensitivities, and is well suited for analysis of plant materials, e.g., (Koosaletse-Mswela et al., 2015; Mesjasz-Przybyłowicz and Przybyłowicz, 2002).

Proton beams were accelerated at low energy (1.90 MeV), with a 1.4 MeV Tandetron tandem accelerator (Cockroft-Walton type manufactured by General Electric). The proton beam of 1 x 1 mm crosses a 7.8-μm-thick kapton foil window before entering the sample chamber and striking the sample. The sample chamber is evacuated to low vacuum to avoid air signal and x-ray absorption. A Canberra Si(Li) detector (detector resolution at the 5.9 keV line is 168.0 eV) is placed at 47° from the normal of the sample surface, which is oriented at 45° with respect to the incoming proton beam. No filters were used in

front of the detector for the low-energy, light-element analyses. Proton current incident on the sample was ~0.5 nA.

PIXE was used to measure element concentrations of atomic number 11 (sodium) and greater in pieces of wood used for preparation of laboratory ash. Spectra were acquired from areas ~1 x 1 mm. Each spectrum was acquired for a total of 20,000 counts (approximately 5 to 7 minutes). The PIXE data were processed with the GUPIX software (www.physics.uoguelph.ca/PIXE, updated 2005). The PIXE spectra showed peaks for Na, Mg, Al, Si, P, S, Cl, K, Ca, and minor Fe. The NIST biological reference material Bovine Liver (SRM-1577) was used for calibration of the PIXE data.

Sections of wood for PIXE analysis were cut and filed flat and smooth. Sanding was not used as grains from the sandpaper became embedded in the wood and contributed to the PIXE spectra. Multiple points were analyzed on each section of wood (Fig. 2, Table 1). For Tree A, spectra were acquired from the bark (PV1a and PV2a) towards the pith. For Tree B, spectra were acquired from five points (PV3a to PV3e) along a 5-cm-section of wood: this piece was taken approximately halfway between the pith and bark of the 30-cm-diameter log.

Scanning electron microscopy and Powder x-ray diffraction

Scanning electron microscope (SEM) images and energy-dispersive x-ray spectra (EDX) were acquired with a JEOL JXA-8530F Hyperprobe. Ash was sprinkled onto a Be planchette and coated with ~5 nm of amorphous carbon. Qualitative EDX spectra were acquired at 10 kV and 10 nA; low accelerating voltage and current were used as some of the ash grains were beam sensitive. An EDX spectrum of the C-coated Be planchette showed an intense Be Kα peak and weak C and O Kα peaks, followed by a low-intensity, featureless Bremsstrahlung continuum. The EDX spectra were used as a guide to help interpret the powder x-ray diffraction (XRD) patterns.

Powder XRD spectra were acquired with a Rigaku D\Max-IIB powder diffractometer employing Cu Kα radiation. Samples were scanned from 5° to 65° 2θ, step size of 0.02°, and with count times ranging from 2 to 20 s per step. Laboratory ash was packed into Al holders for X-ray analysis. The ash collected in the field was more variable in appearance and so representative pieces were deposited onto a single-crystal low-background quartz slide. Mineral identification was undertaken with the JADE v7.0 XRD analysis software and guided by the elemental information provided by EDX and PIXE. A qualitative estimate of mineral concentration was based on overall peak intensities and divided into three categories: X – major, where all the peak intensities and d-spacings in the experimental pattern matched those of a mineral in the Powder Diffraction File (PDF); m – medium, are minerals identified from the most intense reflections

only; and, t – trace, are minerals tentatively identified based on only a few intense reflections. Identification of minerals at minor and trace amounts was facilitated by simulating the patterns of the major minerals present, and subtracting the simulated patterns from the experimental pattern. The EDX and PIXE data were important for the interpretation of the XRD patterns: for example, the laboratory ash often shows a medium-intensity reflection near 30.2° 2θ (Cu Kα) that matches the most intense reflection for natrite (Na_2CO_3) and arcanite (K_2SO_4). However, no discrete Na-rich particles were encountered during the SEM-EDX work, instead K- and S-rich particles were found, consistent with the 30.2° reflection arising from arcanite.

RESULTS

Wood Chemistry and mineralogy

PIXE spectra acquired from Tree A and B show well-resolved peaks for Mg, K, and Ca, which are typically present at >1000 ppm (Table 1). Some areas from Tree A (branches PV1 and PV2) show P, S, and Cl above 1000 ppm. The bark from Tree A (PV2a) has the highest concentrations of Ca, to 6.1 wt%, which correlates with the large numbers of Ca oxalate clusters visible with an optical microscope. Below the bark in the PV2 section, Cl, Mg, and K increase in concentration towards the pith, whereas P is more variable. Apart from the high S content of the PV1 bark (sample PV1a), the S concentrations vary little across each of the three wood samples. For example, S in PV2 is 495±70 ppm. Concentrations for Na, Al, Si, and Fe are less reliable as their counts are near levels of detection (see not in Table 1). Magnesium concentrations correlate with S, suggesting that Mg is present in part as the sulfate, and K correlates with Cl suggesting KCl is present. The K – Cl association is also consistent with wood leaching experiments showing Cl and K readily removed by washing with water (Werkelin et al., 2010). Element concentrations from PV3 for Mg, Cl, K, and Ca do not vary significantly from the average for the five points analyzed: these averages are lower than those for PV1 and PV2.

The paloverde woods show large variations in the major ash-forming element concentrations between different parts of the wood, and in particular old versus younger wood (Table 1). In general, the smaller branches and bark show higher concentrations of ash-forming elements than the mature wood (Table 1), consistent with previous findings, e.g., (Werkelin et al., 2011; Werkelin et al., 2005; Zárubová et al., 2015). Wood from different species and in particular different parts of the same tree show large variations in element concentrations, e.g., (Garvie et al., 2015; Martins et al., 1999; McClenahen et al., 1989; Wang and Dibdiakova, 2014; Werkelin et al., 2011; Werkelin et al., 2005; Werkelin et al., 2010; Zárubová et al., 2015). For example, Werkelin et al. (2011) showed an

order of magnitude difference in Ca, Mg, and K concentrations between wood, bark and twigs of a Scandinavian spruce tree, with lowest concentrations in the wood.

However, comparisons of the paloverde element concentrations with published wood element data is likely uninformative, as wood shows wide element ranges, but with little consensus on the mechanisms or reasons for this range. For example, K varies from an average of 235 ppm in Scandinavian spruce (Werkelin et al., 2011), between 1000 and 4,000 ppm for willow (*Salix* spp.) and poplar wood (*Populus* spp.) from the Czech Republic (Zárubová et al., 2015), to an average of 10,700 ppm in sacred fir (*Abies religiosa*) trees outside Mexico City (Calva-Vázquez et al., 2006). In addition, K can show significant spatial variations measured radially along a tree with rings of different ages, e.g., (Martins et al., 1999). However, in general the paloverde concentrations for Na, Al, Si, P, S and Fe fall within published ranges for wood, but the concentrations for Mg, Cl, K, and Ca are at or above the upper ranges of typical published values.

Powder x-ray diffraction patterns from pieces of cut and polished wood from Tree A showed reflections for whewellite ($CaC_2O_4.H_2O$) only. Whewellite reflections were absent from the interior wood of Tree B (the same sample analyzed by PIXE), though rare clusters were visible with optical microscopy.

Laboratory Ash

Production of ash typically took around two hours starting from ~500 g of dried wood. Temperature measurements taken during the flaming period, after the propane burner was extinguished, were typically above 600° C and locally to 1000° C. Smoldering temperatures were consistently between 350° and 500° C. Ash masses for PV1, PV2, and PV3 were 6.1 wt%, 5.3 wt%, and 3.0 wt% of the starting wood, respectively.

Smoldering is a gentle process producing soft, porous ash "pseudomorphs" of wood (Fig. 1d). These pseudomorphs preserve the macro-wood structure including growth rings, rays, and vessels. SEM images of the PV3 ash are dominated by particles with skeletal, vesicular, thread-like, and flow-like morphologies (Fig. 3). Grains with flow-like morphologies are common (Fig. 3a): their EDX spectra are dominated by K, Ca, C, and O, with minor but variable Mg, P, S, Cl, and Na. Though qualitative, elemental ratios are K:Ca of 2:1, with relative C and O Kα peak intensities consistent with that measured from C-coated calcite. These particles are brighter in backscattered secondary electron (BSE) images compared with the majority of the other particles, which have dominant but variable K and Mg, with minor Ca, Cl, P, S, and Na. Some particles have relative C and O Kα peak intensities consistent with CO_3. Grains with fractal

morphologies (Fig. 3b) are common and dominated by K and O, variable C, and minor Mg: these particles are relatively beam stable suggesting they are not hydrated. Grains with euhedral outlines (Fig. 3c) are rare. These grains are dominated by Ca, with relative C and O Kα peak intensities consistent with CO_3. Particles with Mg:O near 1:1 and minor K, Si, and P are common, consisting of grains to 80 μm long with a cracked surface (Fig. 3d). Though weak peaks for S, P, and Cl were detected with the dominant particle types, no discrete particles were found that contained these elements as major elements. No silicates were found.

The powder XRD patterns of the laboratory ash varied depending on the size of the logs and length of time exposed to the atmosphere. Fresh ash from Tree B (PV3) is dominated by fairchildite, with reflections from nine additional minerals including KOH, K_2CO_3, and periclase (Fig. 4, Table 2). Reflections for calcite are minor to absent. This ash is hygroscopic. For example, a sample exposed to air of ~40% relative humidity (RH) increased in mass by 33% over a three day period. This mass increase was accompanied by mineralogical changes as revealed by powder XRD. Reflections for KOH and K_2CO_3 disappeared within a few hours exposure to air and peaks for baylissite, $K_4H_2(CO_3)_3 1.5H_2O$, $K_2CO_3.1.5H_2O$, and brucite appeared, together with several reflections that could not be matched to known materials (Fig. 5). In order to simulate the effects of the lights rains on the laboratory ash, samples of Tree B (PV3) ash were wetted with a few milliliters of distilled water forming a stiff paste and then air dried. These samples showed a reduction in the intensity of fairchildite reflections accompanied by an increase in intensity of calcite reflections and formation of kalicinite and $K_2CO_3.1.5H_2O$. Washing Tree B ash in water reduced the mass by 51 wt%, leaving a white powder dominated by periclase and broad reflections from magnesian calcite. Evaporation of the supernatant from the ash washing gave a white crystalline solid dominated by $K_4H_2(CO_3)_3 1.5H_2O$ and $K_2CO_3.1.5H_2O$, and eight additional Ca-Mg salts with a range of anions including hydroxide, hydrated carbonate, sulfate, and chloride (Table 2).

The higher ash mass from Tree A (PV2) wood compared to the PV3 wood is consistent with the higher concentrations of ash-forming elements determined by PIXE (Table 1). The PV2 ash contained similar particle types as in the Tree B ash, though the EDX analyses were more challenging because few grains were larger than the electron probe size of ~1 μm. The K-Ca carbonate occurs as thin, <1 μm wide, grains with rounded and vermiform morphologies. Small clusters of KCl cubes are present along with a rare Ca-K-Mg phosphate and clusters of euhedral grains with Ca and O only. XRD patterns of ash from the medium-sized log (Tree A, PV2) shows intense peaks for fairchildite, lime, and calcite, together

with less intense reflections for arcanite, potassium phosphate, langbeinite, and possible $K_2CaP_2O_7$ (Fig. 4). Twig ash is dominated by calcite with minor fairchildite. No silicates were identified in any ash.

Field Ash

Fresh ash collected in the burn area is soft and friable. Ash colors from Tree 1 (Fig. 1c) and 2 range from snow white to grey (N9.5/ to N7/ on the Munsell Neutral value scale): charcoal pieces are rare in the ash. SEM-EDX show the same particles types as in the laboratory ash with flow-like morphologies (Fig. 6a) and dominated by K:Ca of 2:1, with relative C and O Kα peak intensities matching that from CO_3, and consistent with fairchildite. Unlike the fairchildite grains from the laboratory ash, those from the May 15th ashes are cracked and appear "expanded" (Fig. 6a). XRD patterns from multiple samples of Tree 1 and 2 ash were dominated by various proportions of fairchildite, calcite, lime, and periclase (Fig. 7, Table 3). The ash varied from patterns dominated by fairchildite and periclase with minor calcite, to ones with major calcite, lime, and fairchildite. Bütschliite was found as a minor component only in the ash with trace amounts of lime.

Ash collected on May 24th, the day following light rains (0.7 cm), had formed a brittle slag-like crust with a botryoidal morphology. Similar ash crusts have been noted in the field, e.g., (Balfour et al., 2014; Bodí et al., 2014). XRD patterns from the crust are dominated by calcite, with minor but variable amounts of fairchildite, sylvite, kalicinite, baylissite, magnesian calcite, magnesite, and $K_2CO_3.1.5H_2O$ (Table 3). Further light rains fell near the end of May. Ash crust collected in mid June is dominated by calcite, with sparse patches of honey-colored to pale purple, rounded pinnacles of arcanite. Over the following year, the ash crusts dispersed and by 2014, the few remaining deposits were restricted to ash-filled tree stumps. These deposits are dominated by calcite with minor whewellite and nesquihonite. In one stump, nesquihonite formed grains to 4 mm composed of radiating sprays of elongated prismatic crystals (Fig. 8).

Discussion

Wildland fires typically initiate through flaming combustion, which is visually dramatic occurring at high temperature (>1000° C): these fires burn the small, easily combustible materials such as leaves, litter, and small branches, e.g., (Bodí et al., 2014; Rabelo et al., 2004). Flaming sets the stage for smoldering of larger combustible materials such as stumps, logs, and downed branches, which can smolder for days to weeks (Bodí et al., 2014; Carvalho et al., 2002; Ohlemiller, 1985; Rabelo et al., 2004). Wood smoldering is a complex physico-chemical process (Anca-Couce et al., 2012; Ohlemiller, 1985), involving

dehydration (<100° C), oxidation and pyrolysis (<400° C), followed by char oxidation at higher temperatures (e.g., ~500° C), leaving a dominantly inorganic residue of ash, e.g., (Anca-Couce et al., 2012; Bodí et al., 2014; Carvalho et al., 2002; Daouk et al., 2015). Smoldering rates are fairly constant proceeding on the order of 0.5 to 5 cm/h (Carvalho et al., 2002; Rabelo et al., 2004): the rate is largely governed by the porosity of the char, which typically has a higher surface area than the starting material due to pore formation. Char oxidation is the principal heat source in most self-sustaining smolder propagation reactions; this heat drives the lower-temperature wood dehydration, oxidation, and pyrolysis reactions. Char is combusted through pyrolytic gasification (Ohlemiller, 1985), by chemisorption of oxygen with formation of CO and CO_2. The formation of ash "pseudomorphs" after wood (Fig. 1d) is testament to the gentleness of the smoldering reaction. The end result of smoldering is char oxidation leaving a residue of ash dominated by inorganic minerals.

The dominant ash cations, K, Ca, and Mg, derive from essential macronutrients in plants (Canti, 2003; Fromm, 2010). The ash-forming elements (Table 1) are associated as water-soluble salts, minerals, and organically bound elements (Werkelin et al., 2010). Calcium not sequestered in Ca oxalates is deposited mainly in the cell wall. However, Ca oxalates are common in most plants, e.g., (Brown et al., 2013) and references therein), and are argued to be the primary source of calcite in plant ash, based partly on the presence of calcite pseudomorphs after Ca oxalates (Canti, 2003; Shahack-Gross and Ayalon, 2013; Werkelin et al., 2011). Magnesium in wood is divided roughly between water soluble (40% leached) and organically bound components (60% leached), whereas K is dominantly water soluble (75% water leached) (Werkelin et al., 2010). The ash mineralogy depends on the ratios of the dominant ash-forming elements and the burn temperature (Liodakis et al., 2005; Wang and Dibdiakova, 2014; Werkelin et al., 2011).

The primary mineralogy of the paloverde wood was dictated by the relative ratios of the dominant ash-forming cations (Tables 1, 4). Bark from Tree A shows an abundance of whewellite crystals, resulting in Ca being the most abundant ash-forming cation (Tables 1, 4), hence the ash formed under smoldering conditions is primarily calcite. Tree A stem wood (PV2) has an average Ca:K ratio of 1:1.2, and the ash mineralogy was dominated by fairchildite, with variable amounts of lime, arcanite, langbeinite, periclase, and traces of other minerals (Table 2). When K:Ca is >2 and Ca oxalates are rare, then the XRD patterns were dominated by fairchildite, with only minor calcite. The absence of calcite and dominant fairchildite in Tree B ash implies that most available Ca reacted with K during ash formation. Whewellite is rare in Tree B (PV3) wood, so the

source of Ca in fairchildite is likely from Ca organically bound in the cell walls and intracellular Ca (Fromm, 2010; Werkelin et al., 2010; White and Broadley, 2003).

Fairchildite was first described and defined as a mineral in “fused wood-ash stones” (Milton and Axelrod, 1947), though their composition was determined earlier (Englis and Day, 1929). These stones commonly occurred within trunks of standing and partly burned trees. Fairchildite was subsequently identified in 16 plant ashes (Liodakis et al., 2005; Yusiharni and Gilkes, 2012). As shown above, the presence of this mineral in part depends on the initial K to Ca ratio in the wood, and on the burn temperature (Liodakis et al., 2005). For example, fairchildite in *Olnea europaea* ash is only present at smoldering temperatures, i.e., ~600° C. At higher temperatures, it is absent and lime and K carbonates occur. These observations are consistent with thermal data showing that fairchildite melts at ~800° C before decomposing to K_2CO_3 and CaO (Winbo et al., 1998).

As well as fairchildite, Milton and Axelrod (1947) also defined and described the wood-ash mineral bütschliite, with the composition $K_3Ca(CO_3)_2.3H_2O$, named after Johann Adam Otto Bütschli (1848 – 1920) [Note, in the literature this mineral is also spelt buetschliite and butschliite]. They reported that bütschliite formed from fairchildite through wetting and slow hydration in air, which subsequently decomposed to calcite on further weathering. This mineral was then described from Canadian tree ash (Dawson and Sabina, 1957; Mandarino and Harris, 1965). However, in 1966 the name bütschliite was used for the dimorph of fairchildite $K_2Ca(CO_3)_2$ (Effenberger and Langhof, 1984; Mrose et al., 1966; Pabst, 1974), and not the material described by Milton and Axelrod (1947). The IMA recognizes bütschliite $K_2Ca(CO_3)_2$ (and cites Milton and Axelrod 1947) but not the hydrated double carbonate with the same name defined by Milton and Axelrod (1947). However, the x-ray data of Milton and Axelrod (1947) and those derived from the structural data for $K_2Ca(CO_3)_2$ (Winbo et al., 1998) are the same, suggesting that the chemical formula of Milton and Axelrod was in error.

Bütschliite was identified in the fresh field ash only (Table 3) and not in the aged or wetted laboratory ash (Table 2). However, the intensity of the bütschliite reflections did not increase with reduction in intensity of the fairchildite reflections, which would have been the case had bütschliite formed from hydration of fairchildite as suggested by Milton and Axelrod (1947). Instead, in this study, aging of laboratory ash showed a decrease in intensity of the fairchildite reflections and appearance of reflections for kalicinite, baylissite, and hydrated potassium carbonates, and increase in intensity of the calcite and magnesian calcite reflections (Table 2, Fig. 5). Interestingly, reports of bütschliite are all from the western US and Canada (Dawson and Sabina, 1957; Mandarino

and Harris, 1965; Milton and Axelrod, 1947) and only fairchildite reported in ash from subtropical regions (Liodakis et al., 2005; Yusiharni and Gilkes, 2012). Mrose et al. (1966) conclude that bütschliite formed from fairchildite in strong KOH solutions derived from leaching of potash-rich ash, though potash (KOH and K_2CO_3) occurs in the laboratory ash but bütschliite does not.

During smoldering, atmospheric oxygen reacts with the surface of the condensed phase at temperatures between 450° and 600°C (Ohlemiller, 1985), compared to flaming fire temperatures of >1000° C. The formation of calcite from whewellite, instead of lime, is consistent with temperatures of between 479° and 684°C, as determined by thermal analysis (Frost and Weier, 2004). Above 684°C, whewellite decomposes to lime. Similarly, calcite is stable to ~600°C, above which it decomposes to lime. Lime in many of the field ash samples, together with calcite, could imply small-scale temperature variations during smoldering above ~680° C. Such temperature spikes were noted during the laboratory ash production where even a light breeze rapidly propelled smoldering temperatures above 700°C. No lime, and only a trace of calcite, was found in the Tree B ash as the Ca not bound to whewellite reacts with K to form fairchildite. Excess K, i.e., not bonded in Ca salts, forms K_2CO_3 and KOH. During ash formation, the Mg does not react significantly with Ca or K and instead forms periclase, consistent with previous studies (Liodakis et al., 2005; Yusiharni and Gilkes, 2012), though traces of langbeinite and K_2MgCO_3 were tentatively identified in trace amounts in some laboratory ash (Table 2). The formation of calcite and fairchildite in the laboratory ash samples are consistent with the low smoldering temperatures measured between 350° and 500° C.

KOH and K_2CO_3 were present only in the laboratory Tree B ash collected while still hot and stored under dry nitrogen atmosphere prior to X-ray analysis. These minerals are highly sensitive to atmospheric exposure and were not detected after a few hours of atmospheric exposure; this air sensitivity is further increased by the fine-grained nature of the mineral grains. This sensitivity would also explain their absence in the field ash, which was collected hours to days after it formed. Concomitant with the disappearance of KOH and K_2CO_3 reflections was the appearance of reflections for baylissite, $K_2CO_3.1.5H_2O$, and $K_4H_2(CO_3)_3.1.5H_2O$. These minerals are water soluble and readily removed by washing with water, and would similarly be rapidly removed by rain.

Periclase occurs in all field and laboratory ash samples ranging from trace to a major component. Similarly, this mineral was found in ash from Australian (Yusiharni and Gilkes, 2012) and Greek (Liodakis et al., 2005) native plants, and lab-produced wood ash from Scandinavia (Wang and Dibdiakova, 2014; Werkelin et al., 2011). The extensive reporting of periclase in wood ash suggests that it is a widespread component of biomass burning. The periclase reflections

from the paloverde are broad, consistent with mean grain size of ~200 nm, even though SEM imaging showed larger grains (Fig. 3d), suggesting that these grains are polycrystalline. This periclase is unaffected by water washing of Tree B ash and occurs in the field ash sampled within approximately one year after formation. However, it is rare to absent in the ash collected several years following the fire; instead nesquihonite is found, suggesting it as a possible weathering product of periclase. Its long-term instability is consistent with periclase dissolution experiments (Baumann et al., 2015), which show rapid transformation of <10-nm-sized particles to brucite, with slower transformation of larger particles.

IMPLICATIONS

The initial paloverde ash mineralogy is dictated primarily by the concentrations of the primary wood cations Ca, Mg, and K. The ash shows diverse mineralogies depending on age of tree burnt, i.e., twigs versus old logs, and age of the ash, which is further modified by length of atmospheric exposure and contact with rain. In addition, the field and laboratory ash showed similarities and differences in their mineralogy; differences are a function of variable conditions dictated in part by oxygen availability, combustion temperature, length of time and type of fuel, and environmental factors such as air moisture content. Comparably, Liodakis et al. (2005) explored ash elemental composition, mineralogy, and alkalinity of six dominant Greek forest species at combustion temperatures of 600°, 800°, and 1000° C. Ash produced at higher temperatures was dominated by simple oxides, carbonates, and sulfates of Ca, Mg, and K, whereas a more complex mineralogy was present at 600° C, though still dominated by the Ca, Mg, K salts. Other studies have also emphasized the mineralogical and physical differences between residues produced by combustion of plant materials in the lab and during wildland fires. For example, Bodí et al. (2011) showed that heating conditions in a furnace do not adequately reflect burning conditions in the field.

Despite the mineralogical differences between the laboratory and field-collected paloverde ash, the weathering products were similar. Fairchildite, produced during smoldering, rapidly altered to calcite and magnesian calcite, even after light rainfall. Soluble salts, such as sylvite and other K-bearing phases are rapidly solubilized into the soil column. Highly air sensitive salts, such as KOH and K_2CO_3, are absent within a few hours or days of formation. Periclase is removed more slowly from the ash layer. It is unaffected by the relatively short-term laboratory weathering, however it was largely absent in field ash collected two years after the fire, and instead nesquihonite was present. Periclase is commonly reported from wood ash, and this study suggests an important role for

biomass burning in Mg cycling. The aged paloverde ash is mineralogically consistent with that found in anthropogenic ash deposits, which is dominated by calcite (Schiegl et al., 1996; Shahack-Gross and Ayalon, 2013; Shahack-Gross et al., 2008). Silica phytoliths are commonly reported in ash and aged ash deposits, e.g., (Corbineau et al., 2013; Gur-Arieh et al., 2014; Schiegl et al., 1996), though no silica or silicates were detected in the paloverde tree ash, consistent with the low Si content of the paloverde wood and absence of silica phytoliths.

This study shows that knowledge of the elemental ratios of Ca, Mg, and K can be used to predict the dominant ash mineralogy prior to weathering. For example, under smoldering conditions, wood with K:Ca>2 will lead to ash dominated by fairchildite. Whereas under similar smoldering conditions, wood with Ca as the dominant cation will form a calcite-rich ash. The paloverde study showed that even under the semi-arid conditions inherent to the study area, the paloverde ash rapidly weathered to calcite with loss of Mg and K. For example, even the minor 0.7 cm of rain in May following the fire was sufficient to decompose the fairchildite and remove the K-bearing salts. This study raises questions regarding the extent to which ash formed under a range of conditions will affect soil properties differently given that ash having a range of initial compositions and properties will rapidly weather in a similar fashion.

ACKNOWLEDGEMENTS

The author is grateful to two anonymous reviewers for their in-depth and thoughtful suggestions and comments. The author gratefully acknowledges the use of facilities within the LeRoy Eyring Center for Solid State Sciences at Arizona State University, and in particular the assistance of Drs. Barry Wilkens with the PIXE and Henrietta Cathey with the SEM/EDX analyses. The author is also grateful to Kim Stone of the Boyce Thompson Arboretum for providing the monthly rainfall amounts.

Table 1. Element concentrations (ppm) in paloverde wood as determined by PIXE from Tree A (PV1 and PV2) and Tree B (PV3).

Wood	Na	Mg	Al	Si	P	S	Cl	K	Ca	Fe
PV1a bark	402*	3677	428	478	535	1024	530	4484	32533	526*
PV1b	n.d	2490	127*	115*	920	684	609	9477	2375	116*
PV1c	281*	3430	259*	94*	781	557	1407	13615	2720	120*
Average[a]		2960	193	105	851	621	1008	11546	2548	118
PV2a bark	n.d	2214	170*	179*	902	604	318	6355	61772	n.d.
PV2b	234*	816	180*	246*	1528	449	712	9383	9152	188*
PV2c	220*	1127	162*	87*	989	378	662	8567	8267	305*
PV2d	218*	1968	137*	125*	1014	455	1311	12114	12522	136*
PV2e	n.d.	2101	192*	157*	522	522	1482	10586	9163	224*
PV2f	262*	2605	157*	211*	549	555	1852	12670	10054	322*
PV2g pith	175*	2296	72*	46*	396	520	2648	17581	9535	196*
Average[a]	195	1819	150	145	833	479	1445	11817	9782	229
PV3a	460*	1532	144*	97*	n.d.	267	511	4002	1553	163*
PV3b	129*	985	68*	47*	n.d.	164*	536	3965	935	81*
PV3c	450*	1460	292*	223*	129*	246	605	5038	1415	185*
PV3d	331*	1949	212*	238*	69*	375	751	6411	1780	69*
PV3e	272*	1541	87*	83*	n.d.	239	633	6076	1219	146*
Average[a]	328	1493	161	138	-	258	607	5098	1380	107

n.d – not detected at limit of detection

* may be present but near limit of detection (LOD) levels

[a] bark analysis not included in the average

LOD given for PV1c. Detection limits for the other wood samples were within 10% of these values – Na 250 ppm; Mg 128 ppm, Al 103 ppm; Si 78 ppm, P 67 ppm; S 52 ppm; Cl 45 ppm; K 58 ppm; Ca 175 ppm; and Fe 112 ppm

627 Table 2. Materials identified by powder XRD in the fresh, aged, and washed laboratory
628 ash.

Mineral	Tree A (PV1) Bark	Tree A, (PV1)	Tree A, (PV2)	Tree B (PV3)	Tree B, aged ash	Tree B, dried paste	Tree B, Washed ash	Tree B, Crystallized supernatant
Lime	t		m					
Calcite	X	X	m-X	t	t	X	X	
Magnesian calcite		M					X	t
Monohydrocalcite								t
Portlandite								m
KOH				m				
K_2CO_3				m				
Arcanite			m	t	t	m		m
Langbeinite			m					
K_2PO_4			t					
$K_2CaP_2O_7$			t					
Fairchildite		m	X	X	X	m		
$K_2Mg(CO_3)_2$				t				
Baylissite					m			m
Periclase	t	m	t-m	t-m	X	X	X	
Magnesite				t				
Brucite					t			
Sylvite		t	t	t	t			m
kalicinite						X		m
$K_4H_2(CO_3)_3\ 1.5H_2O$					m			X
$K_2CO_3\ 1.5H_2O$				t	t	m		X
Trona								m

629 Notes: Qualitative measure of abundance based on peak intensities, t- trace, m – medium, X – major.
630 Where multiple samples were analyzed, the ranges are shown by a "-".
631 arcanite – K_2SO_4, baylissite – $K_2Mg(CO_3)_2.4H_2O$, brucite – $Mg(OH)_2$, calcite – $CaCO_3$, fairchildite –
632 $K_2Ca(CO_3)_2$, kalicinite – $KHCO_3$, langbeinite – $K_2Mg(SO_4)_3$, lime – CaO, magnesian calcite – $(Ca,Mg)CO_3$,
633 magnesite – $MgCO_3$, monohydrocalcite – $CaCO_3.H_2O$, periclase – MgO, portlandite – $Ca(OH)_2$, sylvite –
634 KCl, trona - $Na_3H(CO_3)_2 2H_2O$.
635
636

Table 3. Minerals identified by powder XRD in samples of field ash.

Mineral	Tree1 15May11[a]	Tree2 15May11	24May11	29May11 crust	11Dec12	26June13
Lime	t-m	m-X	m-X			
Calcite	t-m	t-m	m-X	X	X	X
Magnesian calcite						X
Portlandite		m[b]				
Arcanite	t	T	m	m[d]		
K_2PO_4	t					
$K_2CaP_2O_7$	t					
Fairchildite	t-X	m-X	m			
Bütschliite[c]	t	M	m			
Baylissite	t	T	m			T
Periclase	t-m	m-X	t-X	t		T
Magnesite			t			
Nesquihonite					t-m	t-X
Sylvite			m			
Halite	t					
Kalicinite			m			
K_2CO_3 1.5H_2O			t			
Whewellite						t-m

Note: Qualitative estimate of concentration based on overall peak intensities t - trace, m – medium, X – major. Where multiple samples were analyzed, the ranges are shown by a "-"

[a] Date sample collected

[b] only present after six months of aging in air.

[c] identified from reflections defined for "buetschliite" by Milton and Axelrod (1947).

[d] only in isolated spots on the crust

arcanite – K_2SO_4, baylissite – $K_2Mg(CO_3)_2.4H_2O$, bütschliite – $K_2Ca(CO_3)_2$, calcite – $CaCO_3$, fairchildite – $K_2Ca(CO_3)_2$, halite – NaCl, kalicinite – $KHCO_3$, lime – CaO, magnesian calcite – $(Ca,Mg)CO_3$, magnesite – $MgCO_3$, nesquihonite – $MgCO_3.3H_2O$, periclase – MgO, portlandite – $Ca(OH)_2$, sylvite – KCl, whewellite – $CaC_2O_4.H_2O$.

653 Table 4. Relative atomic ratios of the primary ash-forming cations for the

654 paloverde wood.

655 **Sample**	**element**	**ppm[a]**	**wt%[b]**	**at%**	**ratio**
656	Mg	2214	3.2	5.1	0.06
657 PV2 bark	K	6355	9.0	9.1	0.1
658	Ca	61772	87.8	85.9	1
659	Mg	1819	7.8	12.1	0.3
660 PV2 avg	K	11817	50.5	48.7	1.2
661	Ca	9782	41.8	39.2	1
662	Mg	1493	18.7	27.1	1.8
663 PV3 avg	K	5098	64.0	57.8	3.8
664	Ca	1380	17.3	15.1	1

665 [a] ppm concentrations from Table 1.

666 [b] wt% normalized to 100%

667
668
669

Figure captions

Figure 1. **a**) Photograph of stems of a typical paloverde tree. Largest stem is 12 cm diameter. **b**) Section of paloverde branch (sample PV2 in the paper) showing pith, growth rings, vessels (black dots), and bark. Scale bar = 1 cm. **c**) Typical burnt paloverde tree (Tree 1 in the paper) surrounded by snow-white ash. The trees characteristically burnt at the base with the stems falling around the ash-filled stump. Stump is approximately 24 cm diameter. d) Close-up of an ash pseudomorph of paloverde wood (Tree B, PV3) showing growth rings and vessels. Scale bar = 1 cm.

Figure 2. Photograph of the wood samples analyzed by PIXE. PV1 – Tree A, 3-cm branch. PV2 – Tree A, 9-cm branch. PV3 – Tree B, a 5-cm piece taken from approximately half way between the bark and pith of a 30-cm-diameter trunk. The white squares show the approximate locations and areas analyzed by PIXE. The lower-case letters correspond to the PIXE points in Table 1. Scale at bottom of image is in mm.

Figure 3. Backscattered scanning electron microscope (BSE-SEM) images of typical ash particles from Tree B (PV3). (**a**) Fairchildite particle with flow-like morphology and segmented surface. (**b**) Particle with fractal-like network. EDX spectrum shows major peaks for Mg, K, Ca, C, and O. (**c**) Euhedral calcite pseudomorph after whewellite. (**d**) Anhedral grain of periclase. Scale bars = 10 μm.

Figure 4. Representative powder x-ray diffraction patterns from laboratory ash samples from Tree B (PV3) and Tree A (PV2). Minerals matched include P - periclase, MgO; F - fairchildite, $K_2Ca(CO_3)_2$; Ca - calcite, $CaCO_3$; S - sylvite, KCl; K – KOH; Kc - K_2CO_3; L - lime, CaO; Kp - K_2PO_4; KCp - $K_2CaP_2O_7$; Lb - langbeinite, $K_2Mg(SO_4)_3$; and Ar - arcanite K_2SO_4. Unmatched peaks are shown by a “?”. Both patterns have been scaled in the y-direction so as to show the medium- and low-intensity reflections, as a result, the most intense reflection for fairchildite and calcite are cropped.

Figure 5. Powder x-ray diffraction pattern for fresh Tree B (PV3) laboratory ash, thin line ash, compared with the same sample but aged in air for one week (thick red line online). For clarity, the pattern from 5 to 65 ° 2θ is divided into three segments. Minerals matched include P - periclase, MgO; F - fairchildite,

711 $K_2Ca(CO_3)_2$; Ca - calcite, $CaCO_3$; Mc - magnesian calcite, S - sylvite, KCl; Ba -
712 baylissite, $K_2Mg(CO_3)_2.(H_2O)_4$; K – KOH; Kc - K_2CO_3; Br – brucite, $Mg(OH)_2$; Kh -
713 $K_2CO_3 1.5H_2O$; Ar - arcanite K_2SO_4; Kl – kalicinite $KHCO_3$; and Lb - langbeinite,
714 $K_2Mg(SO_4)_3$. Unmatched peaks are shown by a “?”.
715
716 Figure 6. Backscattered scanning electron microscope (BSE-SEM) images of
717 typical ash particles from Tree 1 field ash. (**a**) Fairchildite particle with flow-like
718 morphology and segmented surface. (**b)** Three euhedral calcite pseudomorph
719 grains after whewellite. Scale bars = 10 μm.
720
721 Figure 7. Representative powder X-ray diffraction patterns for Tree 1 and 2 field
722 ash collected on May 15th, prior to rains. P - periclase, MgO; L – lime, CaO; F -
723 fairchildite, $K_2Ca(CO_3)_2$; Ca - calcite, $CaCO_3$; Ba - baylissite, $K_2Mg(CO_3)_2.(H_2O)_4$;
724 Ar - arcanite K_2SO_4 ; Kp – K_2PO_4; and, KCp – $K_2CaP_2O_7$. Unmatched peaks are
725 shown by a “?”.
726
727 Figure 8. Optical photograph of a nesquihonite cluster found in weathered ash in
728 a paloverde tree stump. Scale bar = 0.5 mm.
729

730 References
731
732
733 Alonso-Canas, I., and Chuvieco, E. (2015) Global burned area mapping from
734 ENVISAT-MERIS and MODIS active fire data. Remote Sensing of
735 Environment, 163, 140-152.
736 Anca-Couce, A., Zobel, N., Berger, A., and Behrendt, F. (2012) Smouldering of
737 pine wood: Kinetics and reaction heats. Combustion and Flame, 159(4),
738 1708-1719.
739 Arthur, M.A., Siccama, T.G., and Yanai, R.D. (1999) Calcium and magnesium in
740 wood of northern hardwood forest species: relations to site characteristics.
741 Canadian Journal of Forest Research-Revue Canadienne De Recherche
742 Forestiere, 29(3), 339-346.
743 Balfour, V.N., Doerr, S.H., and Robichaud, P.R. (2014) The temporal evolution of
744 wildfire ash and implications for post-fire infiltration. International Journal
745 of Wildland Fire, 23(5), 733-745.
746 Baumann, S.O., Schneider, J., Sternig, A., Thomele, D., Stankic, S., Berger, T.,
747 Gronbeck, H., and Diwald, O. (2015) Size effects in MgO cube dissolution.
748 Langmuir, 31(9), 2770-2776.
749 Bodí, M.B., Martin, D.A., Balfour, V.N., Santin, C., Doerr, S.H., Pereira, P.,
750 Cerdà, A., and Mataix-Solera, J. (2014) Wild land fire ash: Production,
751 composition and eco-hydro-geomorphic effects. Earth-Science Reviews,
752 130, 103-127.
753 Bodí, M.B., Mataix-Solera, J., Doerr, S.H., and Cerdà, A. (2011) The wettability of
754 ash from burned vegetation and its relationship to Mediterranean plant
755 species type, burn severity and total organic carbon content. Geoderma,
756 160(3-4), 599-607.
757 Brown, S.L., Warwick, N.W.M., and Prychid, C.J. (2013) Does aridity influence
758 the morphology, distribution and accumulation of calcium oxalate crystals
759 in *Acacia* (Leguminosae: Mimosoideae)? Plant Physiology and
760 Biochemistry, 73, 219-228.
761 Calva-Vázquez, G., Razo-Angel, G., RodrÍguez-Fernández, L., and Ruvalcaba-
762 Sil, J.L. (2006) Study of Z > 18 elements concentration in tree rings from
763 surroundings forests of the Mexico Valley using external beam PIXE.
764 Nuclear Instruments & Methods in Physics Research Section B-Beam
765 Interactions with Materials and Atoms, 249, 588-591.
766 Canti, M.G. (2003) Aspects of the chemical and microscopic characteristics of
767 plant ashes found in archaeological soils. Catena, 54(3), 339-361.
768 Carvalho, E.R., Veras, C.A.G., and Carvalho, J.A. (2002) Experimental
769 investigation of smouldering in biomass. Biomass & Bioenergy, 22(4),
770 283-294.
771 Chandler, C., Cheney, P., Thomas, P., Trabaud, L., and Williams, D. (1983) Fire
772 in forestry. Forest fire behavior and effects. John Wiley & Sons, New York.
773 Corbineau, R., Reyerson, P.E., Alexandre, A., and Santos, G.M. (2013) Towards
774 producing pure phytolith concentrates from plants that are suitable for

carbon isotopic analysis. Review of Palaeobotany and Palynology, 197, 179-185.
Daouk, E., Van de Steene, L., Paviet, F., and Salvador, S. (2015) Thick wood particle pyrolysis in an oxidative atmosphere. Chemical Engineering Science, 126, 608-615.
Dawson, K.R., and Sabina, A. (1957) A Canadian occurrence of fairchildite and buetschliite. Canadian Mineralogist, 6, 290-291.
Demeyer, A., Voundi Nkana, J.C., and Verloo, M.G. (2001) Characteristics of wood ash and influence on soil properties and nutrient uptake: an overview. Bioresource Technology, 77(3), 287-295.
Effenberger, H., and Langhof, H. (1984) On the aplanarity of the CO3 group in buetschliite, dipotassium calcium carbonate, $K_2Ca(CO_3)_2$: a further refinement of the atomic arrangement. Acta Crystallographica, C40, 1299-1300.
Englis, D.T., and Day, W.N. (1929) The composition of peculiar clinkers found in snags after forest fires. Science, 69(1797), 605-606.
Etiégni, L., and Campbell, A.G. (1991) Physical and chemical characteristics of wood ash. Bioresource Technology, 37(2), 173-178.
Fromm, J. (2010) Wood formation of trees in relation to potassium and calcium nutrition. Tree Physiology, 30(9), 1140-1147.
Frost, R.L., and Weier, M.L. (2004) Thermal treatment of whewellite - a thermal analysis and Raman spectroscopic study. Thermochimica Acta, 409(1), 79-85.
Garvie, L.A.J., Wilkens, B., Groy, T.L., and Glaeser, J.A. (2015) Substantial production of drosophilin A methyl ether (tetrachloro-1,4-dimethoxybenzene) by the lignicolous basidiomycete Phellinus badius in the heartwood of mesquite (*Prosopis juliflora*) trees. The Science of Nature, 102(18), 1-18.
Gur-Arieh, S., Shahack-Gross, R., Maeir, A.M., Lehmann, G., Hitchcock, L.A., and Boaretto, E. (2014) The taphonomy and preservation of wood and dung ashes found in archaeological cooking installations: case studies from Iron Age Israel. Journal of Archaeological Science, 46, 50-67.
Humphreys, G.S., Hunt, P.A., and Buchanan, R. (1987) Wood-ash stone near Sydney, NSW - a carbonate pedological feature in acidic soil. Australian Journal of Soil Research, 25(2), 115-124.
Humphreys, G.S., Raven, M.D., and Field, J.A. (2004) Wood-ash stone in *Angophora costata* (Gaertn.) J.Britt. following Sydney bushfires. Australian Forestry, 67, 39-43.
Humphreys, G.S., Shakesby, R.A., Doerr, S.H., Blake, W.H., Wallbrink, P., and Hart, D.M. (2003) Some effects of fire on the regolith. In I.C. Roach, Ed. Advances in Regolith, p. 216-220. CRC LEME.
Koosaletse-Mswela, P., Przybyłowicz, W.J., Cloete, K.J., Barnabas, A.D., Torto, N., and Mesjasz-Przybyłowicz, J. (2015) Quantitative mapping of elemental distribution in leaves of the metallophytes *Helichrysum candolleanum*, *Blepharis aspera*, and *Blepharis diversispina* from Selkirk Cu-Ni mine, Botswana. Nuclear Instruments & Methods in Physics

Research Section B-Beam Interactions with Materials and Atoms, 363, 188-193.
Liodakis, S., Katsigiannis, G., and Kakali, G. (2005) Ash properties of some dominant Greek forest species. Thermochimica Acta, 437, 158-167.
Mandarino, J.A., and Harris, D.C. (1965) New Canadian mineral occurrences: I. Eucryptite, pollucite, rozenite, epsomite, dawsonate, fairchildite and bütschliite. Canadian Mineralogist, 8(377-381).
Martins, J.V., Artaxo, P., Ferraz, E.S.B., and Tabacniks, M.H. (1999) Chronological studies of tree-rings from the Amazon Basin using thick target PIXE and proton backscattering analysis. Nuclear Instruments & Methods in Physics Research Section B-Beam Interactions with Materials and Atoms, 150(1-4), 240-247.
McClenahen, J.R., Vimmerstedt, J.P., and Scherzer, A.J. (1989) Elemental concentrations in tree rings by PIXE: statistical variability, mobility, and effects of altered soil chemistry. Canadian Journal of Forest Research-Revue Canadienne De Recherche Forestiere, 19(7), 880-888.
Mesjasz-Przybyłowicz, J., and Przybyłowicz, W.J. (2002) Micro-PIXE in plant sciences: Present status and perspectives. Nuclear Instruments & Methods in Physics Research Section B-Beam Interactions with Materials and Atoms, 189, 470-481.
Miles, T.R., Miles, T.R.J., Baxter, L.L., Bryers, R.W., Jenkins, B.M., and Oden, L.L. (1995) Alkali deposits found in biomass power plants: a preliminary investigation of their extent and nature. Summary Report for National Renewable Energy Laboratory, Golden, Colorado.
Milton, C., and Axelrod, J. (1947) Fused wood-ash stones: fairchildite (n.sp.) $K_2CO_3.CaCO_3$, buetshliite (n.sp.) $3K_2CO_3.2CaCO_3.6H_2O$ and calcite, $CaCO_3$, their essential components. American Mineralogist, 32, 607-624.
Misra, M.K., Ragland, K.W., and Baker, A.J. (1993) Wood ash composition as a function of furnace temperature. Biomass and Bioenergy, 4(2), 103-116.
Mrose, M.E., Rose, H.J.J., and Marinenko, J.W. (1966) Synthesis and properties of fairchildite and buetschliite: Their relationship in wood-ash stone formation. The Geological Society of America, 101, p. 146, San Francisco.
Ohlemiller, T.J. (1985) Modeling of smoldering combustion propagation. Progress in Energy and Combustion Science, 11(4), 277-310.
Pabst, A. (1974) Synthesis, properties, and structure of $K_2Ca(CO3)_2$, buetschliite. American Mineralogist, 59, 353-358.
Rabelo, E.R.C., Veras, C.A.G., Carvalho, J.A., Alvarado, E.C., Sandberg, D.V., and Santos, J.C. (2004) Log smoldering after an Amazonian deforestation fire. Atmospheric Environment, 38(2), 203-211.
Santín, C., Doerr, S.H., Shakesby, R.A., Bryant, R., Sheridan, G.J., Lane, P.N.J., Smith, H.G., and Bell, T.L. (2012) Carbon loads, forms and sequestration potential within ash deposits produced by wildfire: new insights from the 2009 'Black Saturday' fires, Australia. European Journal of Forest Research, 131(4), 1245-1253.
Schiegl, S., Goldberg, P., BarYosef, O., and Weiner, S. (1996) Ash deposits in Hayonim and Kebara caves, Israel: Macroscopic, microscopic and

867 mineralogical observations, and their archaeological implications. Journal
868 of Archaeological Science, 23(5), 763-781.
869 Shahack-Gross, R., and Ayalon, A. (2013) Stable carbon and oxygen isotopic
870 compositions of wood ash: an experimental study with archaeological
871 implications. Journal of Archaeological Science, 40(1), 570-578.
872 Shahack-Gross, R., Ayalon, A., Goldberg, P., Goren, Y., Ofek, B., Rabinovich,
873 R., and Hovers, E. (2008) Formation processes of cemented features in
874 karstic cave sites revealed using stable oxygen and carbon isotopic
875 analyses: A case study at middle paleolithic Amud Cave, Israel.
876 Geoarchaeology-an International Journal, 23(1), 43-62.
877 Thy, P., Yu, C.W., Jenkins, B.M., and Lesher, C.E. (2013) Inorganic Composition
878 and Environmental Impact of Biomass Feedstock. Energy & Fuels, 27(7),
879 3969-3987.
880 Torn, M.S., Trumbore, S.E., Chadwick, O.A., Vitousek, P.M., and Hendricks,
881 D.M. (1997) Mineral control of soil organic carbon storage and turnover.
882 Nature, 389(6647), 170-173.
883 Ulery, A.L., Graham, R.C., and Amrhein, C. (1993) Wood-ash composition and
884 soil pH following intense burning. Soil Science, 156(5), 358-364.
885 Vassilev, S.V., Baxter, D., Andersen, L.K., and Vassileva, C.G. (2013a) An
886 overview of the composition and application of biomass ash. Part 1.
887 Phase-mineral and chemical composition and classification. Fuel, 105, 40-
888 76.
889 Vassilev, S.V., Baxter, D., and Vassileva, C.G. (2013b) An overview of the
890 behaviour of biomass during combustion: Part I. Phase-mineral
891 transformations of organic and inorganic matter. Fuel, 112, 391-449.
892 Wang, L., and Dibdiakova, J. (2014) Characterization of ashes from different
893 wood parts of Norway spruce tree. Chemical Engineering Transactions,
894 37, 37-42.
895 Werkelin, J., Lindberg, D., Bostrom, D., Skrifvars, B.J., and Hupa, M. (2011) Ash-
896 forming elements in four Scandinavian wood species part 3: Combustion
897 of five spruce samples. Biomass & Bioenergy, 35(1), 725-733.
898 Werkelin, J., Skrifvars, B.J., and Hupa, M. (2005) Ash-forming elements in four
899 Scandinavian wood species. Part 1: Summer harvest. Biomass &
900 Bioenergy, 29(6), 451-466.
901 Werkelin, J., Skrifvars, B.J., Zevenhoven, M., Holmbom, B., and Hupa, M. (2010)
902 Chemical forms of ash-forming elements in woody biomass fuels. Fuel,
903 89(2), 481-493.
904 White, P.J., and Broadley, M.R. (2003) Calcium in plants. Annals of Botany,
905 92(4), 487-511.
906 Winbo, C., Rosén, E., and Heim, M. (1998) Thermal analytical study of the
907 decomposition of $K_2Ca_2(CO_3)_3$. Acta Chemica Scandinavica, 52(4), 431-
908 434.
909 Yusiharni, E., and Gilkes, R. (2012) Minerals in the ash of Australian native
910 plants. Geoderma, 189-190, 369-380.
911 Zárubová, P., Hejcman, M., Vondráčková, S., Mrnka, L., Száková, J., and
912 Tlustoš, P. (2015) Distribution of P, K, Ca, Mg, Cd, Cu, Fe, Mn, Pb and Zn

in wood and bark age classes of willows and poplars used for phytoextraction on soils contaminated by risk elements. Environmental Science and Pollution Research, 22(23), 18801-18813.

Figure 1
Mineralogy of paloverde (Parkinsonia microphylla) tree ash

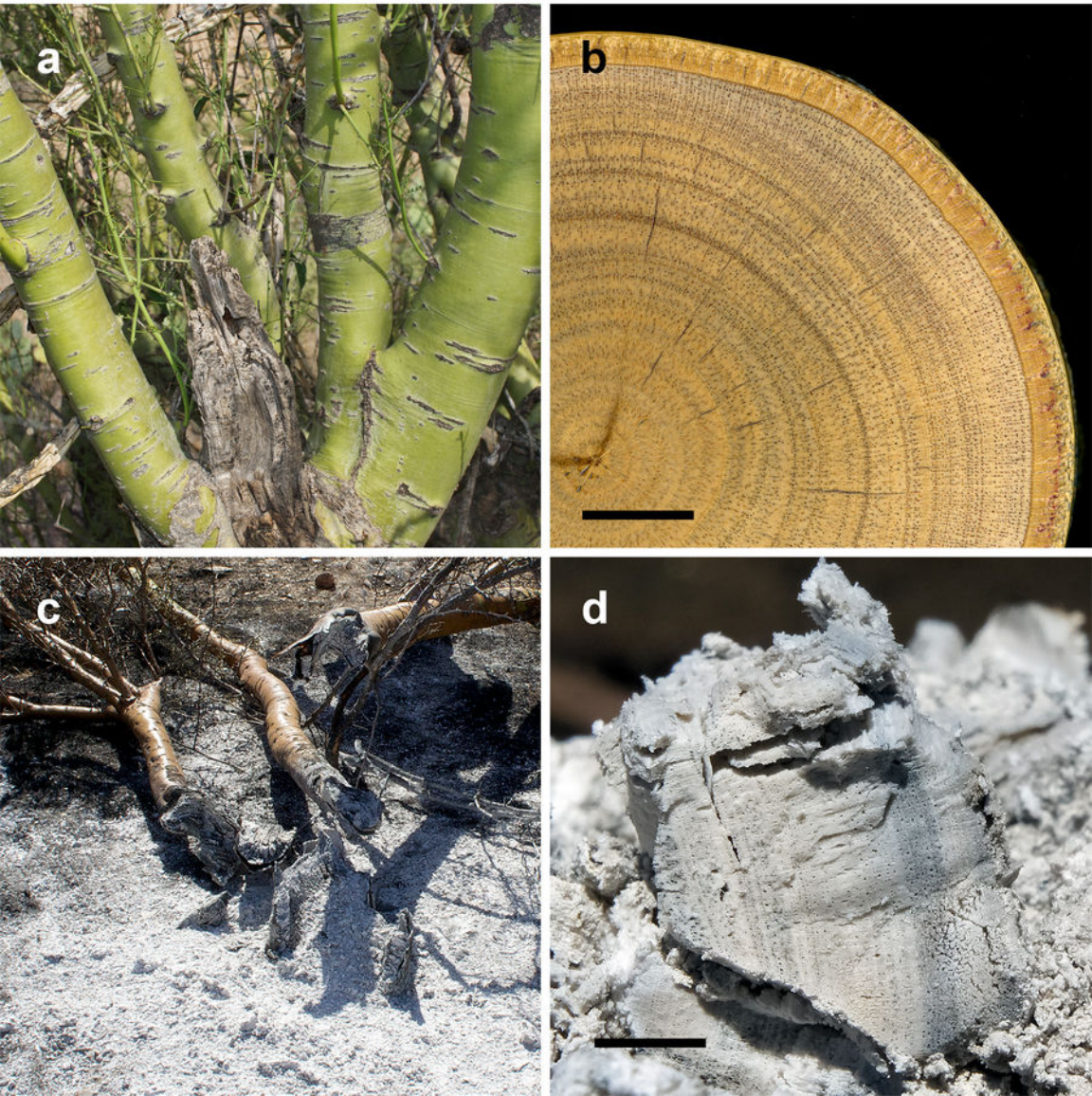

Figure 2
Mineralogy of paloverde (Parkinsonia microphylla) tree ash

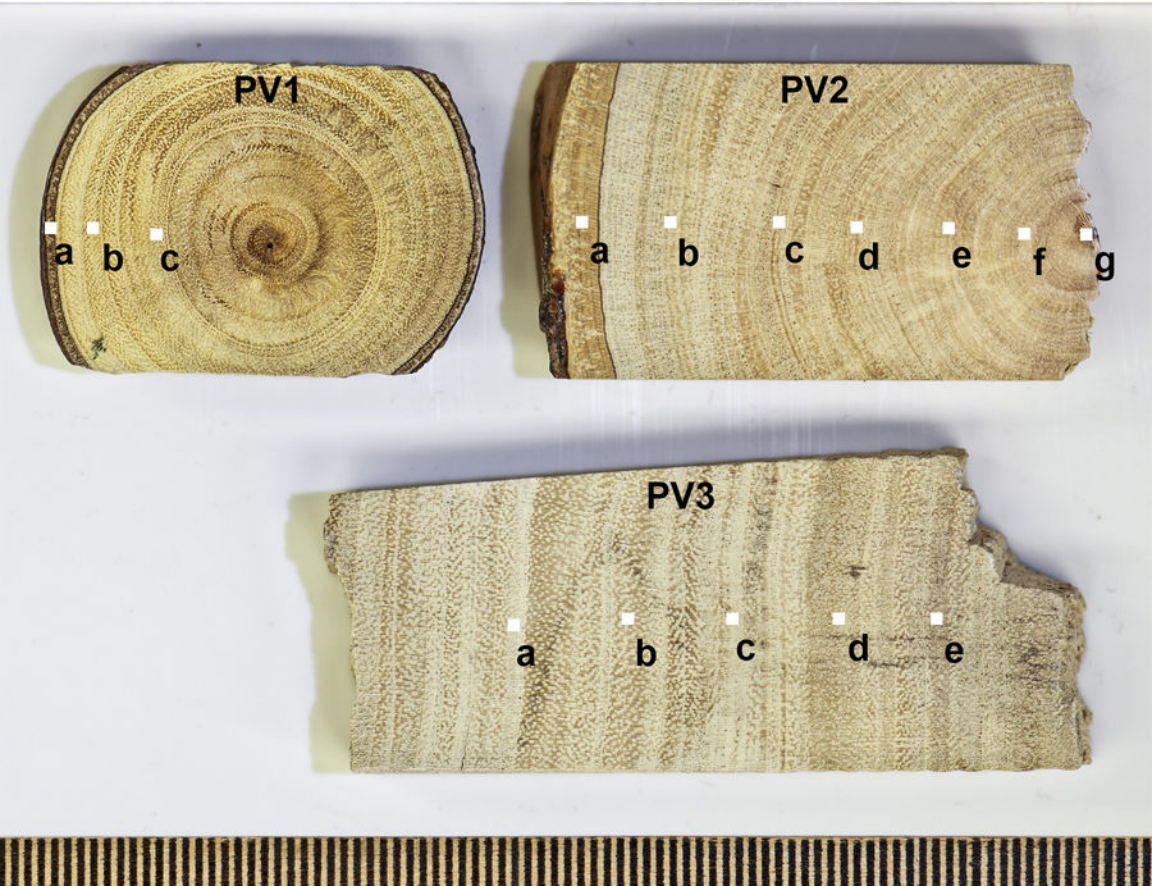

Figure 3
Mineralogy of paloverde (Parkinsonia microphylla) tree ash

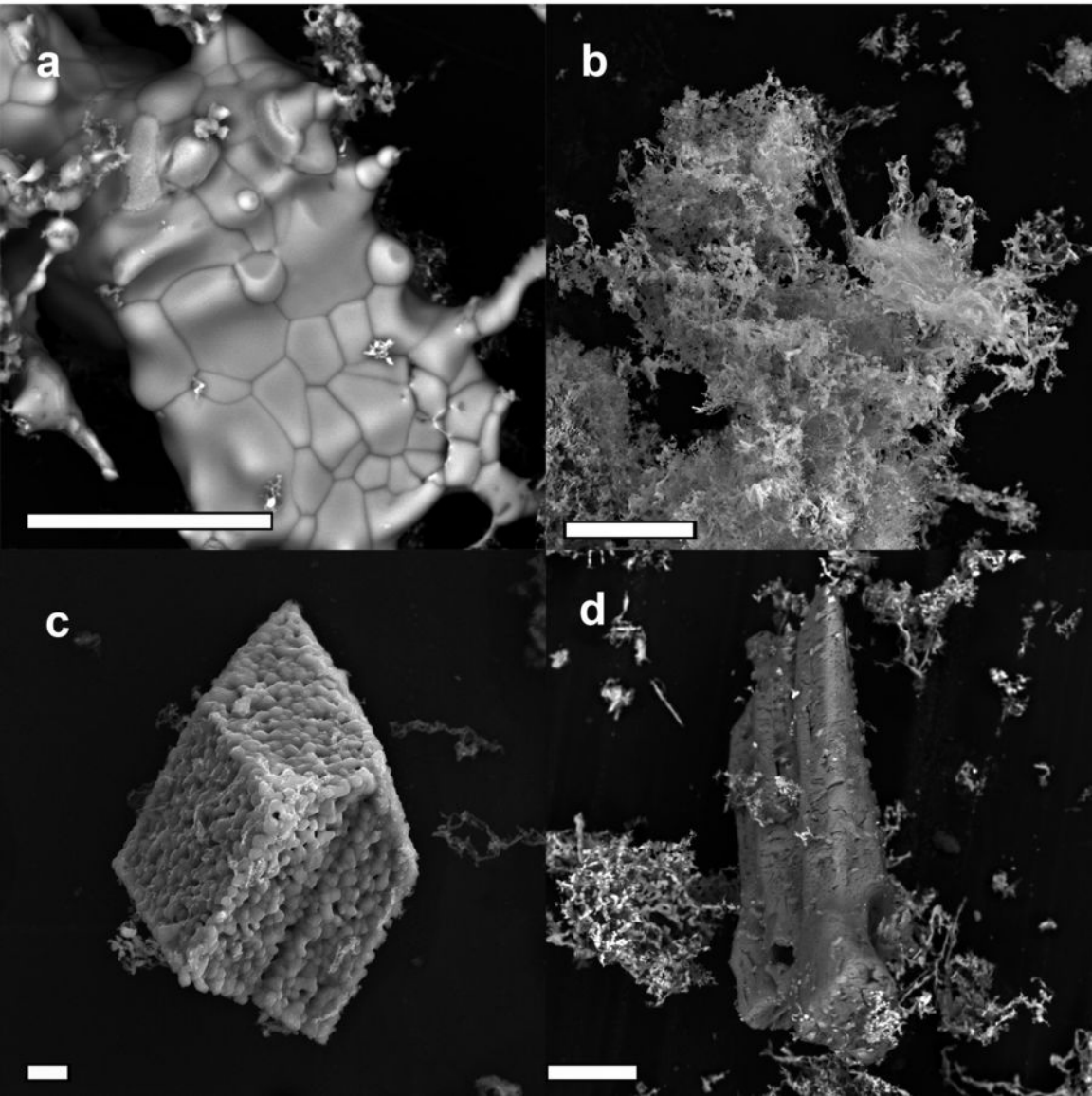

Figure 4
Mineralogy of paloverde (Parkinsonia microphylla) tree ash

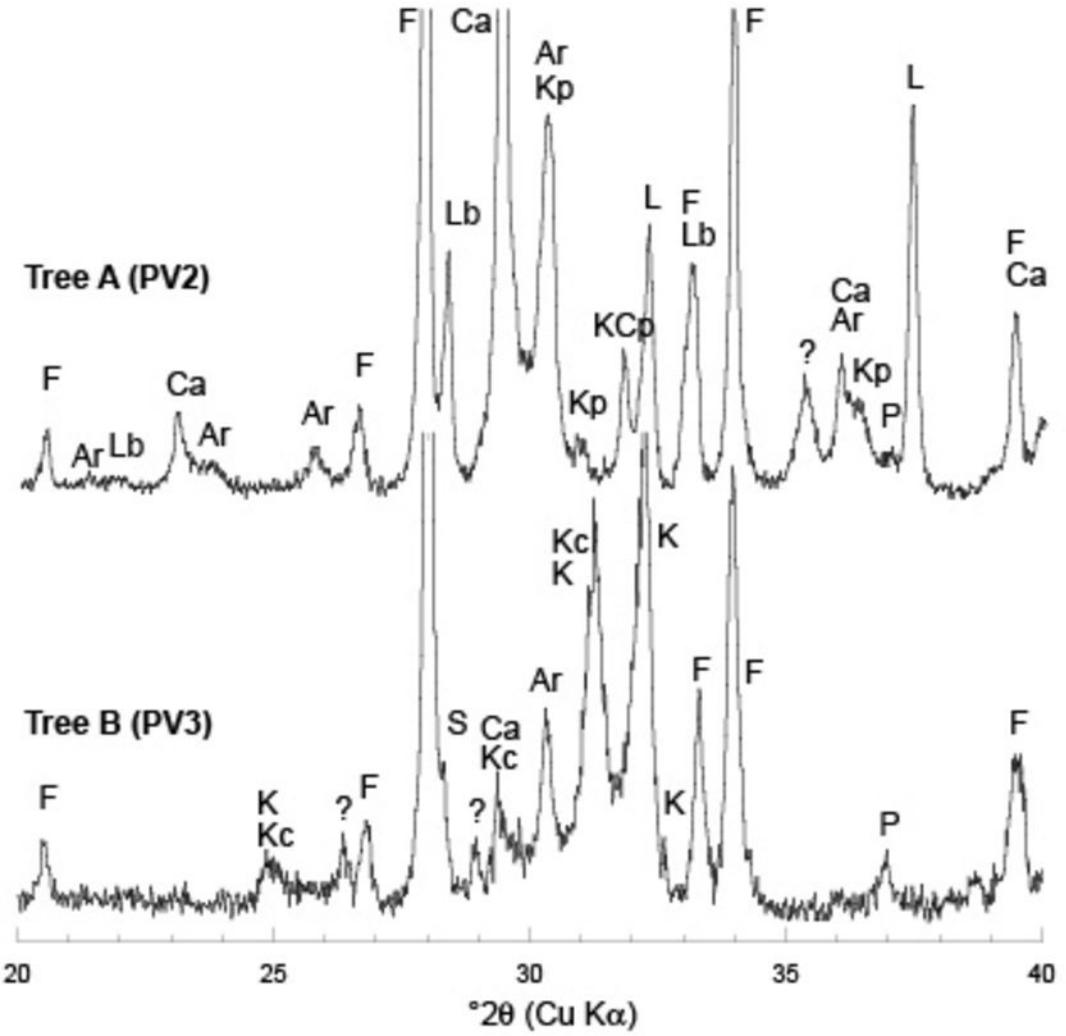

Figure 5
Mineralogy of paloverde (Parkinsonia microphylla) tree ash

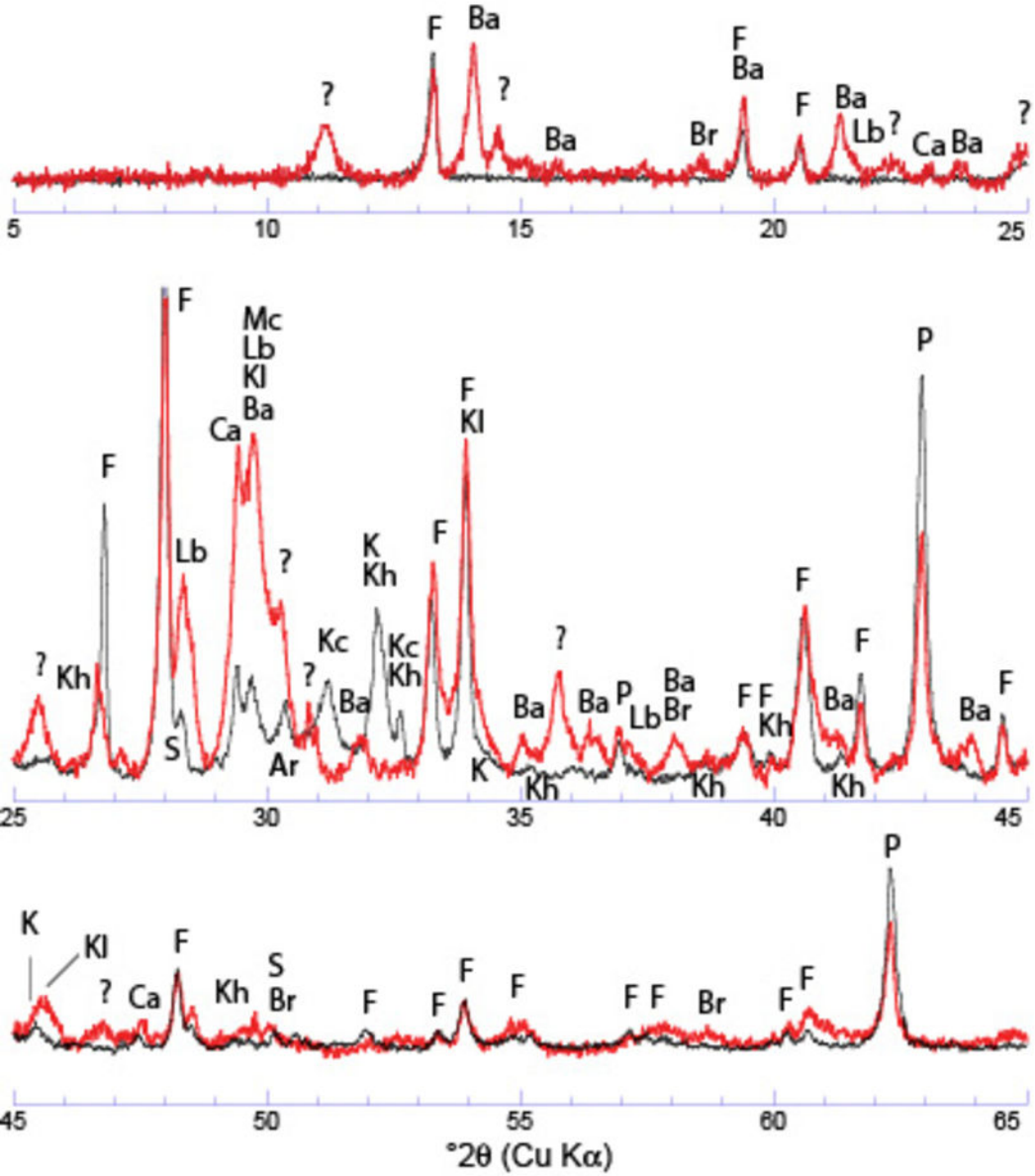

Figure 6
Mineralogy of paloverde (Parkinsonia microphylla) tree ash

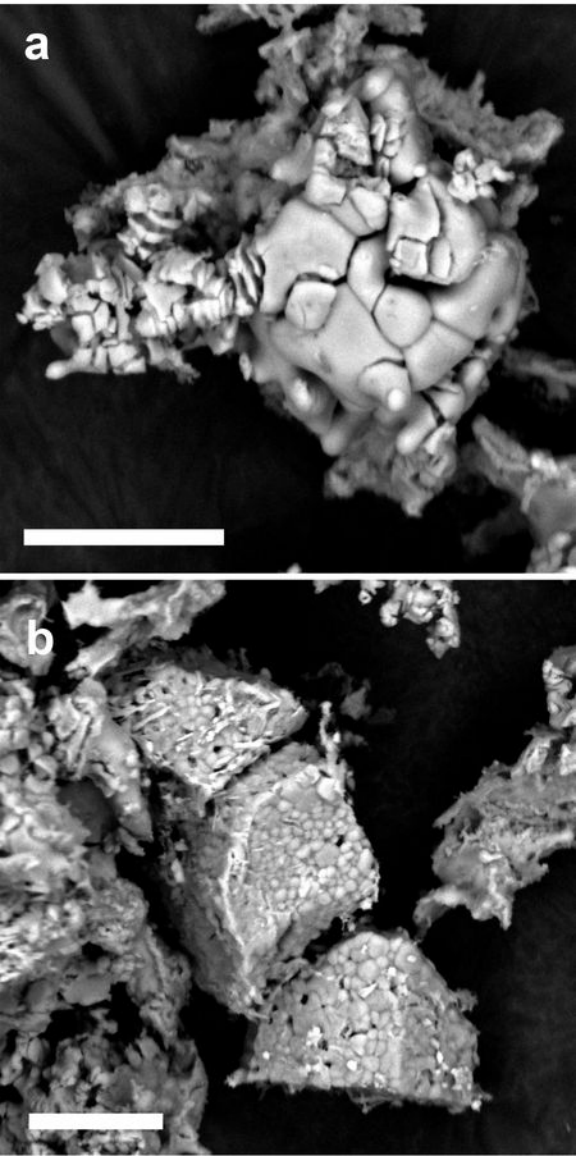

Figure 7
Mineralogy of paloverde (Parkinsonia microphylla) tree ash

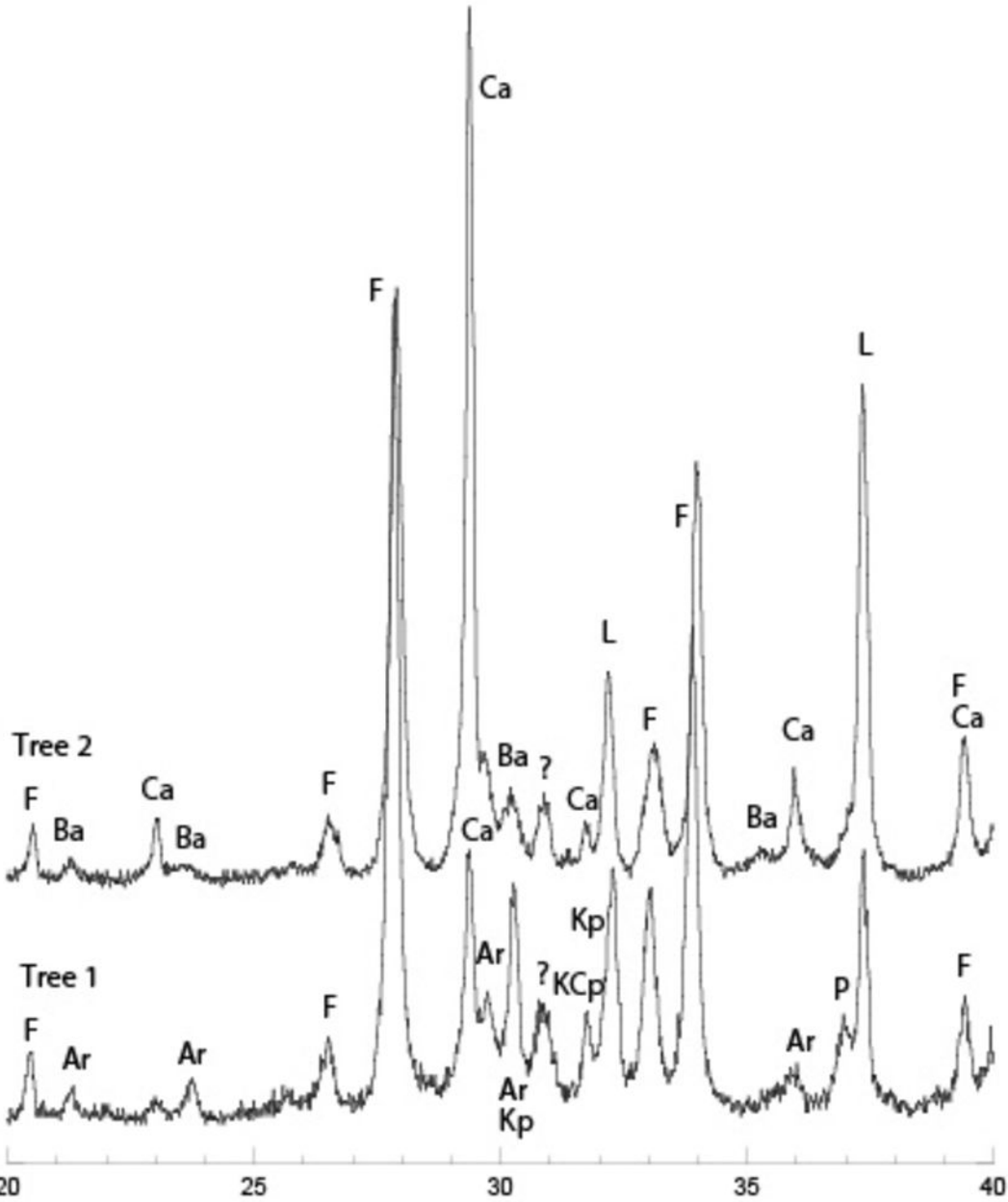

Figure 8
Mineralogy of paloverde (Parkinsonia microphylla) tree ash